Ultrasonics 91 (2019) 161–169

Contents lists available at ScienceDirect

Ultrasonics

journal homepage: www.elsevier.com/locate/ultras

Classification of spot-welded joint strength using ultrasonic signal time-frequency features and PSO-SVM method

Wang Xiaokai[a,b], Guan Shanyue[a,b,c,*], Hua Lin[a,b], Wang Bin[a,b], He Ximing[a,b]

[a] Hubei Key Laboratory of Advanced Technology for Automotive Components, Wuhan University of Technology, Wuhan 430070, China
[b] Hubei Collaborative Innovation Center for Automotive Components Technology, Wuhan 430070, China
[c] College of Mechanical & Power Engineering of China Three Gorges University, Yichang 443002, China

ARTICLE INFO

Keywords:
Spot-welded joint
Ultrasonic detection
Tensile-shear strength
Feature extraction
PSO-SVM

ABSTRACT

Resistance spot welding (RSW) ultrasonic testing signal contains nugget size and internal defect information which can reflect the mechanical property of spot-welded joint. The mechanical property of spot-welded joint is the most direct indicator for evaluation of spot welding quality. In this paper, 100 samples of different quality spot-welded joints are detected by ultrasonic detection technology, then ultrasonic signals are processed by fast Fourier transform (FFT) and wavelet packet transform (WPT). After that, mathematical statistical methods are used to feature extraction for ultrasonic detection signals in time domain, frequency domain, and wavelet domain based on WPT. 100 samples are subjected to tensile-shear tests to obtain the maximum tensile-shear strength (MTSS) that is used as the classification identifier here. Finally, back-propagation (BP) neural network classifier and particle swarm optimization support vector machine (PSO-SVM) classifier are used to classify the MTSS of spot-welded joints and comparing the accuracy of the two classifiers with different number of features. The results show that the PSO-SVM classifier with all 9 features has a good accuracy, which verifies the feasibility and correctness of the spot welding quality classification method proposed in this paper.

1. Introduction

Resistance Spot welding (RSW) has been widely used in welding assembly of automobile sheet metal. The number of the spot welds of a typical family car is about 3000–6000. The quality of spot-welded joints directly affects the reliability and safety of the auto-body. At present, the main methods of detection of spot-welded joints strength are chiseling, tensile-shear test and metallographic experiment. Ultrasonic nondestructive detection technology, which has the characteristics of convenient operation and high detection sensitivity, has been used to detect the spot welds [1,2]. Many researchers analyzed the ultrasonic echo waveform, which was related to the nugget size, to evaluate the spot welding quality. MM Fujita et al. [3] proposed a new ultrasonic measurement with a line-focused probe to evaluate spot welding nugget diameter. Óscar Martín et al. [4] extracted the features of attenuation and peak time spacing in time domain signal and use artificial neural network to classify spot welding quality. Z Chen et al. [5] established the relation between ultrasonic signals and nugget diameter or relevant maximum shear load, the characteristic value is indicated by the power of signals decomposed in WPT.

The strength of spot welded joint is affected by various factors, such as nugget size, pores, cracks, coarse grains and so on. Ultrasonic time domain signals are always used to estimate the nugget size [6]. The signal features of other factors such as pores, cracks and coarse grains are easily submerged by noise in time domain waveform. However, these factors can be distinguished in frequency domain and wavelet domain. In recent years, some studies have analyzed the signal features of frequency domain and wavelet domain to evaluate the spot welding quality. Liu J et al. [7] used wavelet packet decomposition to extract the time-frequency characteristic of ultrasonic detection signals of the spot weld, and evaluated the weld nugget diameter with these time-frequency characteristics. F.C. Cruz et al. [8] extracted the signal features of the ultrasonic echo waveform of the spot welds based on the discrete Fourier, wavelet and cosine transforms, and classified the spot welds into three defect types. G Zhou et al. [9] analyzed the frequency spectrum characteristic curve of ultrasonic test to evaluate the laser weld width. However, these studies focus on the prediction of spot weld nugget size and internal defects. In practice, the maximum tensile-shear strength (MTSS) of the spot-welded is the most direct parameter for evaluating the quality of welded joints, and has been widely used in research and industry [10]. To predict the TSS of the spot-welded, some researchers monitored electrical parameters such as interelectrode

* Corresponding author at: School of Automotive Engineering, Wuhan University of Technology, Wuhan 430070, China.
E-mail address: gsyawesome@163.com (S. Guan).

https://doi.org/10.1016/j.ultras.2018.08.014
Received 29 May 2018; Received in revised form 13 August 2018; Accepted 15 August 2018
Available online 18 August 2018

voltage, welding current and dynamic resistance. However, the electrical parameters were less sensitive to the strength of spot-welded joints, so predictive results were volatile and show poor reliability [11,12].

Based on the above research, this paper proposes a prediction and classification method about MTSS of spot-welded joints. Mathematical statistics and signal processing methods are used to feature extraction for ultrasonic detection signals. Meanwhile, the MTSS value of all samples are obtained by tensile-shear test. The spot welding quality of all samples are classified into good spot-welded joints, qualified spot-welded joints and unqualified spot-welded joints. Finally, the BP neural network classifier and PSO-SVM classifier are trained to classify the MTSS of spot-welded joints. Comparing the accuracy of the two classifiers with different numbers of features, it shows that the more features are used, the classifier's accuracy increase, and the PSO-SVM classifier is more accurate than traditional BP neural network classifier. The research results have great significance for the quality prediction and nondestructive evaluation of spot-welded joint.

2. Experimental method

2.1. Detection device and method

The 1.6-mm thick dual-phase steel DP590 is widely used in the automotive industry, especially for the primary frame components of car body. DP590 has no yield point elongation compared with traditional high-strength steel, it can contribute to the absorption of more impact energy in the forming process [13]. The chemical composition of this steel is presented in Table 1. The samples are cut into pieces in dimensions of 100 mm × 30 mm, as shown in Fig. 1(b), a total of 100 groups. The spot welding process is resistance spot welding in this paper. JTF-600DN resistance spot welding machine was used in this experiment. The welding parameters of a spot-welded joint are shown in Table 2, and the ultrasonic testing signal is Fig. 5. The electrode tips are a combination of a flat tip and a cone tip, as shown in Fig. 1(c). 100 groups of resistance spot welding specimens are prepared through different welding parameters and welding conditions. The detector is manufactured by Guangzhou Doppler Company, China. The ultrasonic probe's type is 15P6Y-H which means the transducer's nominal frequency and diameter are 15 MHz and 6 mm, as shown in Fig. 1(a). the diameter of delay block is 7.6 mm.

2.2. Tensile-shear test

In this paper, the tensile-shear tests were carried out on the CMT series microcomputer control electronic universal testing machine at a cross-head speed of 2 mm/min, and 1.6 mm suitable shims were used to ensure alignment. The load-displacement curves were recorded separately in the test to determine the tensile shear strength of the specimen and the corresponding fracture failure mode. As shown in Fig. 2, the failure behaviors of three cases were studied during tensile-shear loading condition, which included failure modes: Tearing of Base Metal (mode A), Button Pullout (mode B), Interfacial Failure (mode C). The load-displacement curves for these three failure modes were recorded separately in the test, as shown in Fig. 3. The mode A is broken off from the outer edge of the heat affected zone and near the base metal, and finally tear along the basis material. The mode B is broken off from the inner side of the heat affected zone and near the nugget, showing that the welded joint is pulled out. The mode C is separated from the nugget interface [14]. As shown in Fig. 4, tensile shear strength distribution of 100 samples. The MTSS of spot welding can be divided into three grades: good spot-welded joints (a, $F_a > 19$ kN), qualified spot-welded joints (b, $19 \geq F_b \geq 17$ kN) and unqualified spot-welded joints (c, $F_c < 17$ kN).

Table 1
Chemical composition of DP590 steel.

Chemical element	C	Si	Mn	P	S	Alt
weight %	0.071	0.43	1.84	0.011	0.02	≥0.01

3. Features extraction of ultrasonic detection signal

3.1. Time domain features

Here, average peak spacing $\overline{S}$ and amplitude coefficient Q are chosen as the two time-domain features. Fig. 5 is ultrasonic signal for a spot welded joint with 20.14 kN tensile-shear strength. The average peak spacing of the ultrasonic time-domain waveform reflects the thickness of welding area and depth of indentation. The average peak spacing $\overline{S}$ is defined as:

$$\overline{S} = \frac{V(T_n - T_m)}{n - m} \tag{1}$$

where V is velocity of ultrasonic in material, T_m,T_n is the sampling time spacing of the two peak points of the m th and n th bottom echoes. In oscillogram, the maximum number of wave peaks is 10, while the amplitude of 10 th peaks are very small. For best result, $m = 1, n = 9$ in this study.

As shown in Fig. 5. When the nugget diameter d is less than delay block diameter D, the values of P_a and P_b are proportional to their reflection area. That is to say, with the increase of nugget diameter, P_a increases due to the increasing of the lower plate reflection area, and P_b decreases for the reducing of the upper plate reflection area [6]. Amplitude coefficient Q is used to represent the ratio of amplitude value P_b and P_b, that is:

$$Q = |P_b / P_a| \tag{2}$$

3.2. Frequency domain analysis

FFT method is used to find the frequency components of the ultrasound time domain waveform. As shown in Fig. 6, the ultrasonic frequency spectrum consists of a series of resonant peaks. These resonance peaks are half-wave resonance signals caused by superposition of ultrasonic waves in thin plate. The attenuation of the resonance peak amplitude is due to the scattering of defects inside the spot welding. The resonant frequency distribution reflects the internal defect information of spot welding [15]. During the ultrasonic testing process, the collected detection signals are discrete, and ultrasonic test signal is a discrete sampling sequence. The formula as Eq. (3) for the discrete signal FFT is:

$$F\left(\frac{a}{NT}\right) = \sum_{b=0}^{N-1} P(bT) e^{-j2\pi ab/N} \tag{3}$$

where $P(bT)$ is the ultrasonic detection signal sampling value, N is sampling number, T is sampling time spacing, a is a frequency domain discrete sequence number, b is a time domain discrete sequence number.

In spectrum curve, the frequency of the harmonic component with the highest amplitude is the main spectrum frequency f_m, it represents that the harmonic wave energy of this frequency has the largest influence on the original signal. The maximum spectral amplitude A_m represents the amplitude of the harmonic wave of the main frequency f_m.

Kurtosis represents the characteristic of the peak density distribution curve at the main spectrum frequency f_m by comparing frequency distribution curves with normal distribution curves. A high kurtosis is caused by the extreme difference between the frequency and the main frequency f_m [16]. Kurtosis of frequency $Kurt(F)$ is defined as:

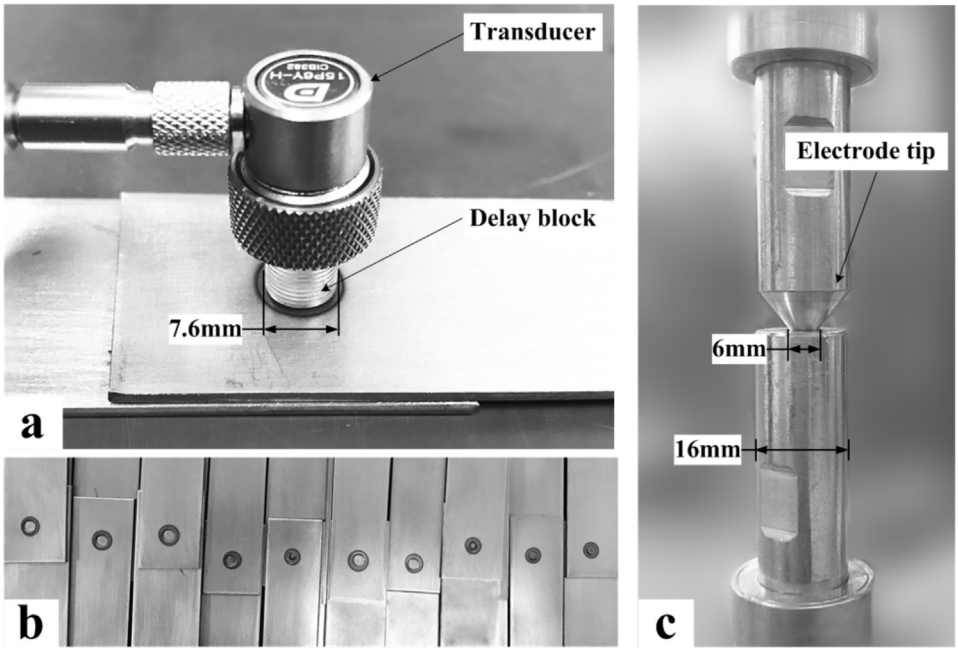

Fig. 1. Ultrasonic detection probe (a); spot welding samples (b); electrode tips of spot welding machine (c).

Table 2
The welding parameters.

Parameters	Squeeze time (s)	Welding current (kA)	Welding time (s)	Electrode force (kN)	Holding time (s)
Values	1	9.5	0.72	2.5	0.6

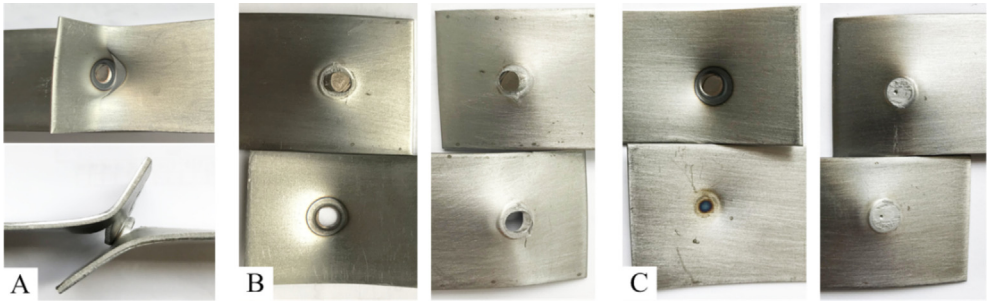

Fig. 2. Tensile-shear failure modes of: mode A, mode B, mode C.

$$Kurt(F) = \frac{\sum_{i=1}^{N}(F_i - f_m)^4 F_i}{\sigma^4 \sum F_i} \quad (4)$$

where F is the frequency in spectrum; σ is the standard deviation value; N is the number of discrete points in the frequency domain.

3.3. Wavelet domain analysis

3.3.1. Wavelet packet transform (WPT)

The actual ultrasonic signal is unstable, which is easy to generate singularity. FFT is single resolution, so it's hard to analyze the singularity of the signal. WPT has good localization feature and multi-resolution analysis, and capacity of detecting local signal mutation. In addition, WPT is a good way to analyze the high frequency bands of frequency resolution, so it is more suitable to analyze ultrasonic signal of time-frequency features. The high-frequency part of ultrasonic signals reflects the information of the material's internal structure and defect information [17,18]. After the processing of WPT, some hidden defect features can be extracted from low frequency bands and high

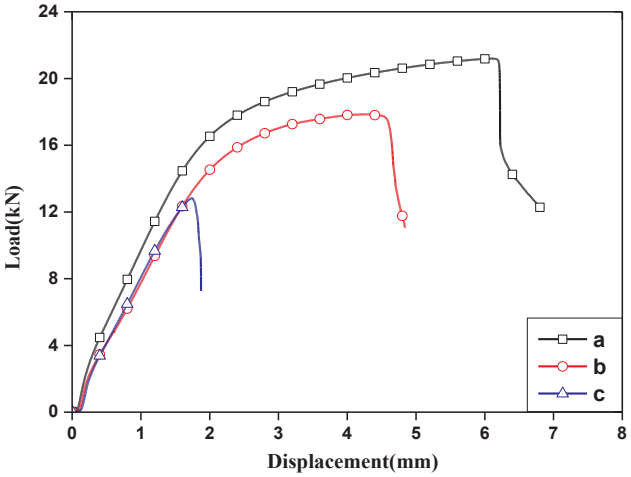

Fig. 3. Load-displacement curves.

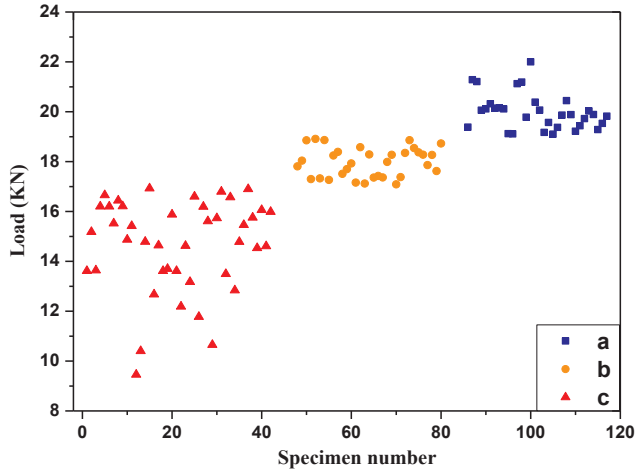

Fig. 4. Tensile-shear strength distribution of 100 samples.

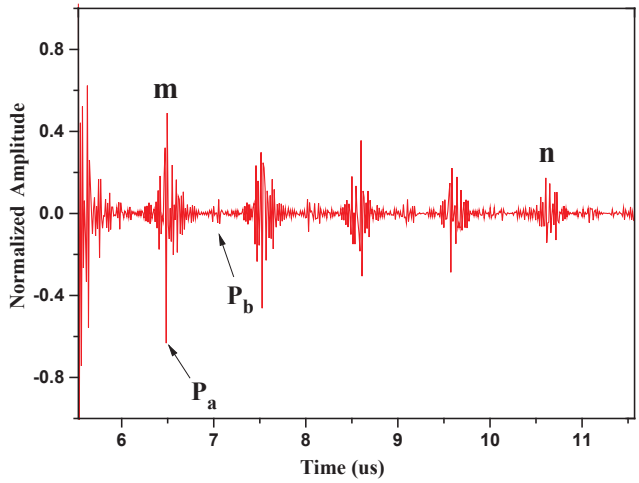

Fig. 5. Ultrasonic original signal of spot welding samples.

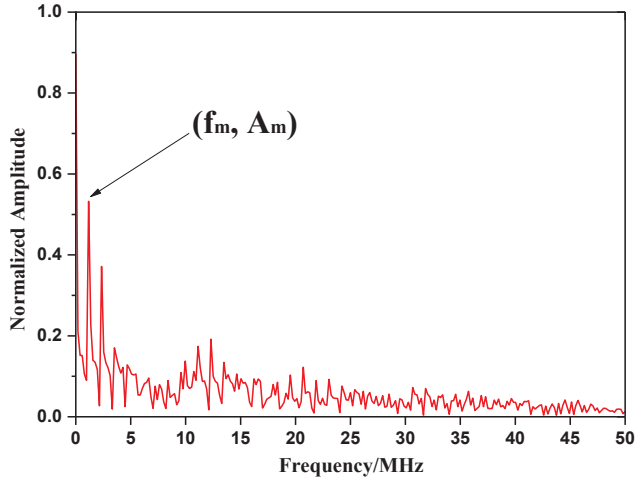

Fig. 6. Spectrum curve of ultrasonic signal after fast Fourier transform.

frequency bands. In this paper, the energy distribution and the attenuation coefficient of each sub-band are chosen as the recognition features. According to the decomposition theory based on orthogonal wavelet packet, the definition of the subspace W_j^n is the closure space of the function $W_n(x)$, and W_j^{2n} is the closure space of the function $W_{2n}(x)$ [19]. Defining function $W_n(x)$ satisfies dual-scale function Eqs. (5), (6):

$$W_{2n}(x) = \sqrt{2}\sum_{k\in z} h(k)W_n(2x-k) \tag{5}$$

$$W_{2n+1}(x) = \sqrt{2}\sum_{k\in z} g(k)W_n(2x-k) \tag{6}$$

where $\{g(k)\} = (-1)^k h(1-k)$ is high-pass filter, $\{h(k)\}$ is low-pass filter, $\{h(k)\}$ and $\{g(k)\}$ are conjugate filters defined in multiresolution analysis [20]. Since Symlets8 (Sym8) wavelet function has better orthogonality, compactness and faster decomposition than other wavelets [21]. Through carry out wavelet packet transform for ultrasonic signal with different layers, when the number of decomposition layers exceeded three, the sub-band signal waveform was seriously distorted and the signal was seriously lost. To improve the resolution, the layers of wavelet packet transform was chosen as 3. The ultrasonic signal is decomposed by Sym8 wavelet function, it is operated by three-layer wavelet packet decomposition to get eight frequency band signals, as shown in Fig. 7.

3.3.2. *Energy average value* $\overline{E}$ *and energy variance* S_E^2

After the interaction between the ultrasonic signal and the defect, the different frequency component of the ultrasonic echo signal changes due to the defect's enhancement or suppression. Different frequency band signals have different energy changes in the process of material propagation, which is reflected in each frequency band energy after wavelet packet decomposition [22]. Defining the energy of each equidistant band is E_j, as Eq. (7), and total energy of high-frequency bands $(S_2 \cdots S_8)$ is E, energy average value $\overline{E}$ is calculated as Eq. (8) shows:

$$E_j = \sqrt{\int |Z_j(t)|^2 dt} = \sqrt{\sum_{n=1}^{N_j} |P(n)|^2} \tag{7}$$

$$E = \sqrt{\sum_{j=1}^{7} E_j^2},\ \overline{E} = E/7 \tag{8}$$

where $Z_i(t)$ is layer j band signal, $P(n)$ is the amplitude of the discrete point of layer j band signal, N_j is sampling number of layer j band signal. The high-frequency bands after the WPT of ultrasonic signal contain more defect feature information [5]. In order to describe the defect features accurately and improve the classification accuracy, the energy variance of high-frequency bands S_E^2 is used to represent the feature value, that is:

$$S_E^2 = \frac{1}{7}\sum_{j=1}^{7} (E_j - \overline{E})^2 \tag{9}$$

3.3.3. *Attenuation coefficient average value* $\overline{\alpha}$ *and variance value* S_α^2

The attenuation of ultrasonic signal mainly includes two aspects: one is the ultrasonic absorption and scattering effect in material, the other is the multiple reflection and transmission effect in sheet structure [23]. So the attenuation coefficient can reflect the internal structure of spot-welded joints. Ultrasonic signal attenuation is mainly related to the distance of ultrasonic transmission and the frequency of ultrasonic signal. That is to say, the attenuation of ultrasonic signal is discrepant in different frequency bands. The attenuation coefficients α_j of high-frequency bands are calculated as Eq. (10), average value $\overline{\alpha}$ and variance value S_α^2 is used to represent the feature value, that is:

$$\alpha_j = -\frac{10}{(x_2 - x_1)h}\log_{10}\left|\frac{P_j(x_2)}{P_j(x_1)}\right| \tag{10}$$

$$\overline{\alpha} = \alpha_j/7 \tag{11}$$

$$S_\alpha^2 = \frac{1}{7}\sum_{j=1}^{7} (\alpha_j - \overline{\alpha})^2 \tag{12}$$

where $P_j(x_1)$, $P_j(x_2)$ are the amplitudes of the x_1 th and x_2 th received waves in the j layer band signal, h is the thickness of the plate, $h = 1.6$ mm, $x_1 = 6$, $x_2 = 2$.

In summary, a total of 9 features are extracted of ultrasonic

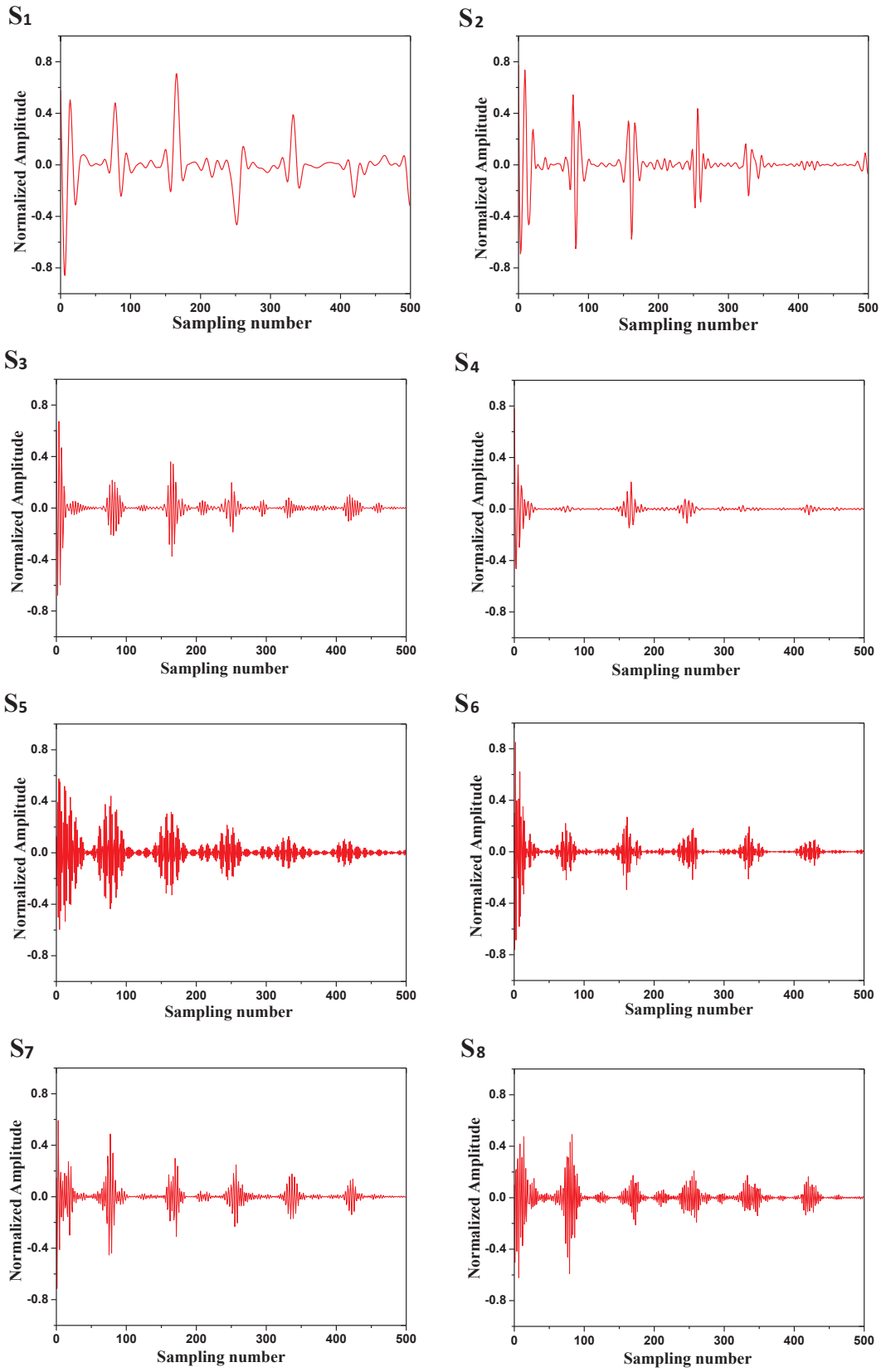

Fig. 7. Three-layer wavelet packet decomposition of ultrasonic signals to get eight frequency band signals ($S_1 \cdots S_8$).

Table 3
Ultrasonic detection signal features extraction of spot welding samples and MTSS.

Number	Time domain		Frequency domain			Wavelet domain				MTSS
	$\bar{S}\,(mm)$	Q	f_m(MHz)	A_m	$Kurt$	$\bar{E}$	$S_E{}^2$	$\bar{\alpha}\,(dB/mm)$	$S_\alpha{}^2$	$Load$(kN)
1	2.95	0.541	1.172	0.221	0.361	0.442	0.374	5.39	3.48	13.62
2	2.87	0.355	0.780	0.381	0.443	0.617	0.475	2.81	2.59	15.18
3	2.51	0.470	1.172	0.284	0.798	0.514	0.321	1.44	1.73	17.81
4	2.43	0.236	1.367	0.492	0.331	0.527	0.437	3.22	2.42	19.38
5	2.21	0.113	1.367	0.849	0.410	0.891	0.859	2.03	0.45	21.21
6	2.88	0.154	1.172	0.477	0.213	0.246	0.227	6.17	4.77	13.64
7	2.92	0.407	1.172	0.654	0.549	0.640	0.571	4.52	4.29	18.04
8	2.74	0.363	1.172	0.568	0.554	0.735	0.593	2.62	0.96	20.06
9	2.36	0.106	1.367	0.971	0.424	0.904	0.579	2.48	0.72	20.32
10	2.79	0.174	1.172	0.793	0.595	0.731	0.765	1.94	0.67	20.14
11	2.94	0.394	0.780	0.262	0.576	0.348	0.311	4.37	3.02	16.20
⋮	⋮	⋮	⋮	⋮	⋮	⋮	⋮	⋮	⋮	⋮
⋮	⋮	⋮	⋮	⋮	⋮	⋮	⋮	⋮	⋮	⋮
99	2.59	0.265	0.780	0.394	0.341	0.357	0.329	4.33	2.86	16.66
100	2.64	0.189	1.367	0.496	0.349	0.875	0.462	2.56	1.99	18.72

detection signal, it includes 2 features of time domain, 3 features of frequency domain, 4 features of wavelet domain, as shown in Table 3.

4. Classification

4.1. Support vector machine (SVM)

SVM is the method that one maps the data into a higher dimensional input space and one constructs an optimal separating hyperplane in this space. Based on the structural risk minimization principle and capacity concept with pure combinatorial definitions, the quality and complexity of the SVM solution does not depend directly on the dimensionality of the input space [24]. SVM has good robustness and do not require fine-tuning. It can construct functions in a wide variety of functions and is one of the most effective methods for solving practical problems [25]. Kernel function, which is proposed and developed in the study of SVMs, is a new way of constructing nonlinear map. Assume that the two input sample sets are:

$$U = \{(x_1, y_1), \cdots, (x_i, y_i)\} \in (X \times Y)^l \tag{13}$$

where $x_i \in R^n$, $y_i \in Y = \{1, 2, 3\}(i = 1, 2, \cdots, l)$, the three output targets are set as 1, 2, 3. l is the number of the input sample, n is the dimension of the input sample. SVM uses the optimal hyperplane to classify the samples, as P: $\boldsymbol{\omega}\cdot\boldsymbol{x} + b^* = 0$. It makes the 3 kinds of data in T to be correctly distinguished and maximizes the distance from the sample to the classification surface, this is, $||\omega||^2$ is the smallest. Where, $\boldsymbol{\omega}$ is the normal vector of the optimal classification surface, b^* is the classification threshold [26]. The nonlinear SVM classifier mathematical formula is shown as follows:

$$\begin{cases} \min\varphi(\omega, \varepsilon) = \frac{1}{2}||\boldsymbol{\omega}||^2 + c\sum_{i=1}^{l}\varepsilon_i \\ s.\ t.\ y_i(\boldsymbol{\omega}\cdot\boldsymbol{x} + b^*) \geq 1-\varepsilon_i,\ \varepsilon_i \geq 0;\ i = 1, 2, \cdots, l \end{cases} \tag{14}$$

where ε_i is relaxation factor, it indicates that the sample training allows a small number of erroneous samples. c is penalty parameter, it represents the degree of punishment for wrong samples. Select the appropriate kernel function $H(x_i, x)$ and suitable penalty parameter c to structural decision function, as Eq. (15) shows:

$$f(x) = sgn\left[\sum_{i=1}^{l} y_i\alpha_i^* H(x_i, x) + b^*\right] \tag{15}$$

where $0 \leq \alpha_i^* \leq c$. Radial basis function (RBF) has fewer parameters than other kernel functions, so it has a faster learning speed. Furthermore, RBF has a strong locality and better classification ability [27]. As a result, radial basis function (RBF) is used in this study. The feature space of a kernel function is infinitely dimensioned, so that a finite sample can be linearly separable after being transformed into this space [28]. $H(x_i, x) = \exp(-g||x_i - x||^2)$, where $g = \partial^{-2}$ is the important parameter of the kernel function, so decision function, as Eq. (16) shows:

$$f(x) = sgn\left(\sum_{i=1}^{l} y_i\alpha_i^* \exp(-g||x_i - x||^2) + b^*\right) \tag{16}$$

4.2. Optimization of SVM parameters based on particle swarm optimization (PSO) algorithm

PSO is a population-based search algorithm that is initialized with a population of random solutions, called particles. That is, each individual particle in the search space has a velocity, which is dynamically adjusted through searching the best example of particles in solution space [29]. The particle with high classification accuracy and a small number of features produce a high fitness value. PSO algorithm has the fast search speed and high efficiency, and it can be easily adopted for parallel processing [30]. Therefore, to improve the SVM performance, PSO algorithm is chosen as an optimization technique to optimize the input feature subset selection and the SVM parameters

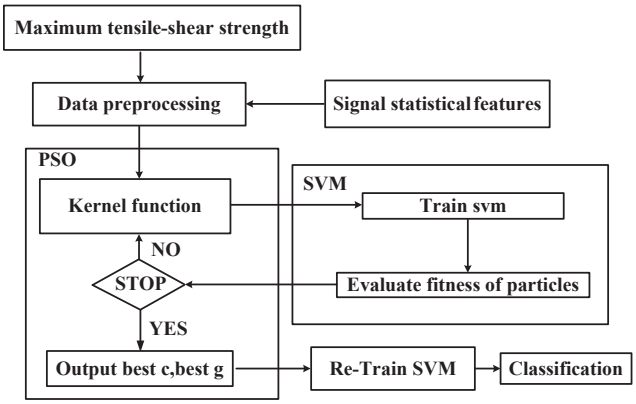

Fig. 8. The architecture of the proposed PSO-based parameter optimization algorithm for the SVM classifier.

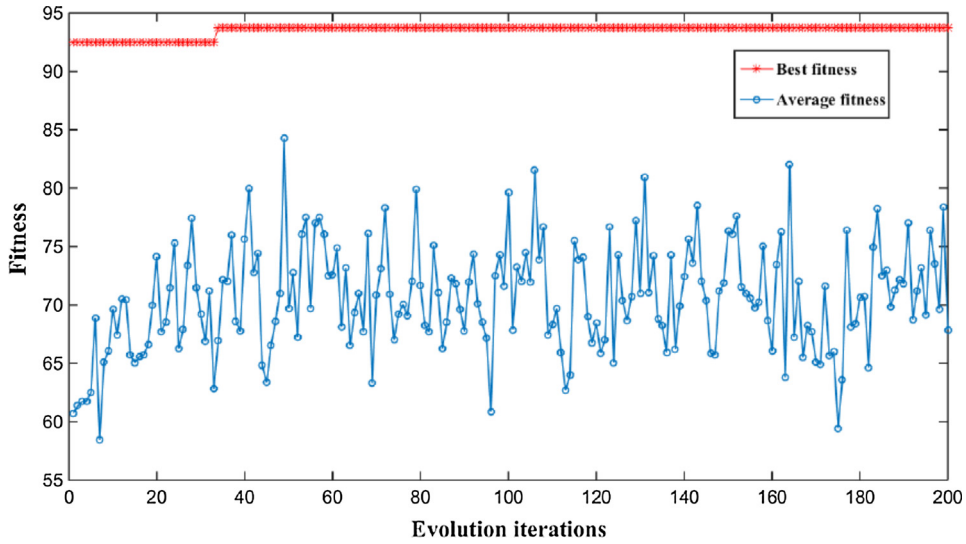

Fig. 9. The best fitness evolution of the fitness function.

setting simultaneously. The penalty parameter c and RBF kernel function parameter g (c & g) main affect the accuracy of SVM classifier. The architecture of the proposed PSO-based parameter optimization algorithm for the SVM classifier, as shown in Fig. 8.

First, the ultrasonic testing signals of spot-welded joint are classified into three categories according to the three grades of the MTSS obtained in Tensile-shear test. Signal processing and statistical analysis methods are used to extract features and they are stored in database files. Each set of data is 10-dimensional. The first dimension is the category identifier, and the last 9 dimensions are the signal feature values. From the data, 80 sets of data were randomly selected as training data and 20 sets were used as test data. Normalization of all data and use the normalized mapping as Eq. (17) follows:

$$f: x \to y = \frac{x - xmin}{\max(x) - \min(x)} \tag{17}$$

where $x, y \in R^n$, the effect of normalization is that the original data is normalized to the range [0,1].

PSO algorithm is used to find penalty parameter c and RBF kernel function parameter g (c & g), the final fitness curve is shown in Fig. 9. The PSO-SVM neural network classifier results are shown in Fig. 10(a). 19 of the 20 test samples are accurately identified and the correct rate is 95%. Traditional BP classifier is also adapted to compare with the PSO-SVM classifier, as shown in Fig. 10(b), 14 of the 20 test samples are accurately identified and the correct rate is 70%. It can be seen that the PSO-SVM classifier performs better than BP classifier, and the recognition accuracy rate is significantly improved.

From Table 4, it can be seen that the classification accuracy of POS-SVM classifier are higher than BP classifier. Because there are so many parameters to be optimized for the BP neural network, and the convergence rate is slow. Another reason is that BP is easy to generate local extremum problems when the sample sizes are small; in this case, the solution obtained by the BP is not the global optimal solution, resulting in lower accuracy [31]. The SVM solve the classification problem by maximizing the margin between the separating hyper-plane and the data [32]. In addition, the SVM overcomes the problems of local minimum value effectively. Especially when dealing with the finite sample problem, it still shows good performance. The 20 sets of test data in this study are small sample events, while SVM has advantages in small sample processing. Therefore, the test results show that the accuracy of the SVM classifier is higher than BP classifier. From Table 4, it can be seen that the classification accuracy of both BP and POS-SVM classifier are higher in the case that the input features are only in wavelet domain, which is higher than that in time domain and frequency domain. There are two main reasons for this result. On the one hand, the rough surfaces and grain size variations of spot-welded joints will cause ultrasonic signal noise. Some details of the defects such as size and space orientation are submerged by noise [33]. When the signal is decomposed by WPT, the noise can be excluded, and the time domain characteristics of signals at all scales are preserved [34]. WPT have the characteristic of multi-scale decomposition, the overall condition and details of the signal can be observed, including grain size, location and size of defects. By means of mathematical statistics, the overall time-frequency features distribution of ultrasonic signals is studied. On the other hand, all of the features selected in this paper are related to the strength of spot-welded joints, so the more input parameters, the accuracy of neural network classifier are higher. From the experimental data, the PSO-SVM classifier with all 9 input features is the best of all, which has the highest classification accuracy of 95%. So when the four wavelet domain features are used as input parameters, the classifier's accuracy is higher than two time-domain features and three frequency-domain features.

5. Conclusion

This article proposed a classification method of maximum tensile-shear strength (MTSS) of spot-welded joint. Signal processing and mathematical statistics methods were used to extract features of spot welding ultrasonic detection signals as input parameters, and tensile-shear tests were used to obtain the MTSS as output parameters to establish a PSO-SVM classifier. Using PSO algorithm to find the SVM parameters (c & g) can effectively improve PSO-SVM classifier's performance. The spot welding quality can be effectively classified into three classes by the PSO-SVM classifier. Feature selection is of great importance in neural network classifier, effective features can improve the accuracy of classifier. From the classification results, the classifier with the features in wavelet domain is higher than that in time domain and frequency domain, and it indicated that the input features in wavelet domain have ampler information of the spot welding quality. By comparing BP classifier and PSO-SVM classifier in this study, the results show that PSO-SVM classifier is more accurate and stable than traditional BP classifier.

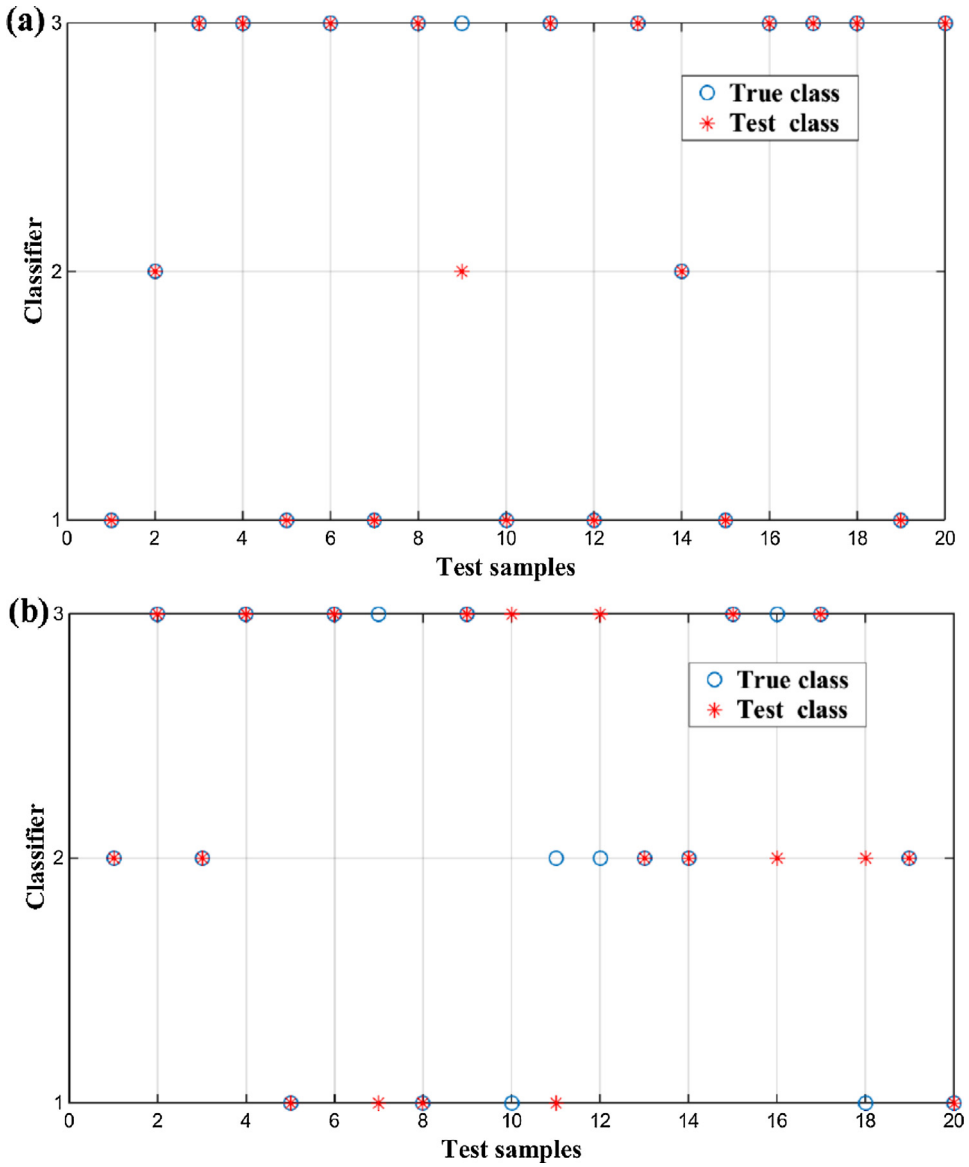

Fig. 10. PSO-SVM classification results (a); BP neural network classification results (b).

Table 4
The accuracy of PSO-SVM and BP classifier.

Input feature type	BP classifier		POS-SVM classifier	
	Correct classification number	Correct classification rate	Correct classification number	Correct classification rate
Time domain	10	50%	11	55%
Frequency domain	9	45%	10	50%
Wavelet domain	13	65%	17	85%
All features	14	70%	19	95%

Acknowledgements

This work was supported by National Key Research and Development Plan of China (No. 2018YFB1106503), Team Development Program of Ministry of Education of China (No. IRT_17R83), the 111 Project (No. B17034) and the Science and Technology Support Program of Hubei Province (No. 2015BCE083). The authors would like to acknowledge the supports.

Appendix A. Supplementary material

Supplementary data associated with this article can be found, in the online version, at https://doi.org/10.1016/j.ultras.2018.08.014.

References

[1] B.S. Ben, S.H. Yang, C. Ratnam, et al., Ultrasonic based structural damage detection using combined finite element and model Lamb wave propagation parameters in composite materials, Int. J. Adv. Manuf. Technol. 67 (5–8) (2013) 1847–1856.

[2] T. Wang, C. Wang, G. Xu, Ultrasonic scanning inspection research on Resistance spot welding joints, Insight - Non-Destructive Testing Condition Monitor. 56 (11) (2014) 617–621(5).
[3] M.M. Fujita, M.M. Ueno, C. Iwamoto, et al., Ultrasonic evaluation of spot welding nugget diameter with a line-focused probe, Welding World 53 (11–12) (2009) R281–R289.
[4] Óscar Martín, M. López, F. Martín, Artificial neural networks for quality control by ultrasonic testing in resistance spot welding, J. Mater. Process. Technol 183 (2) (2007) 226–233.
[5] Z. Chen, Y. Shi, B. Jiao, et al., Ultrasonic nondestructive evaluation of spot welds for zinc-coated high strength steel sheet based on wavelet packet analysis, J. Mater. Process. Technol. 209 (5) (2009) 2329–2337.
[6] Y.K. Song, L. Hua, X.K. Wang, et al., Research on the detection model and method for evaluating spot welding quality based on ultrasonic a-scan analysis, J. Nondestr. Eval. 35 (4) (2016).
[7] J. Liu, G.C. Xu, X.P. Gu, et al., Ultrasonic test of resistance spot welds based on wavelet package analysis, Ultrasonics 56 (2014) 557–565.
[8] F.C. Cruz, E.F. Simas Filho, M.C. Albuquerque, et al., Efficient feature selection for neural network based detection of flaws in steel welded joints using ultrasound testing, Ultrasonics 73 (2017) 1–8.
[9] G. Zhou, G. Xu, J. Liu, et al., Assessment of laser weld width based on time and frequency domains of ultrasonic testing signals, J. Mater. Process. Technol. 251 (2017).
[10] N. Kahraman, The influence of welding parameters on the joint strength of resistance spot-welded titanium sheets, Mater. Des. 28 (2) (2007) 420–427.
[11] M. Stölting, C. Handschin, B. Attila, Quality evaluation by classification of electrode force patterns in the resistance spot welding process using neural networks, Proc. Inst. Mech. Eng. Part B J. Eng. Manuf. 218 (11) (2004) 1513–1524.
[12] M. El-Banna, D. Filev, R.B. ChinnamOnline, Qualitative nugget classification by using a linear vector quantization neural network for resistance spot welding, Int. J. Adv. Manuf. Technol. 36 (3–4) (2008) 237–248.
[13] B. Wang, L. Hua, X. Wang, et al., Effects of multi-pulse tempering on resistance spot welding of DP590 steel, Int. J. Adv. Manuf. Technol. 86 (9–12) (2016) 2927–2935.
[14] M. Asme, Ultimate strength and failure mechanism of resistance spot weld subjected to tensile, shear, or combined tensile/shear loads, J. Eng. Mater. Technol. 125 (2) (2003) 125–132.
[15] J. Liu, G. Xu, X. Gu, et al., Ultrasonic test of resistance spot welds based on wavelet package analysis, Ultrasonics 56 (2015) 557–565.
[16] M. Vejdannik, A. Sadr, Automatic microstructural characterization and classification using dual tree complex wavelet-based features and Bees Algorithm, Neural Comput. Appl. 28 (2016) 1–13.
[17] Y. Chen, A support vector machine approach for classification of welding defects from ultrasonic signals, Nondestruct. Test. Eva. 29 (3) (2014) 243–254.
[18] P. Yang, Q. Li, Wavelet transform based feature extraction for ultrasonic flaw signal classification, Neural Comput. Appl. 24 (3–4) (2014) 817–826.
[19] A. Daamouche, L. Hamami, N. Alajlan, et al., A wavelet optimization approach for ECG signal classification, Biomed. Signal Process. Control 7 (4) (2012) 342–349.
[20] H.G. Yang, Y.S. Zhang, X.M. Lai, An experimental investigation on critical specimen sizes of high strength steels DP600 in resistance spot welding, Mater. Des. 29 (9) (2008) 1679–1684.
[21] B. Yan, S. Goto, A. Miyamoto, et al., Imaging-based rating for corrosion states of weathering steel using wavelet transform and PSO-SVM techniques, J. Comput. Civil Eng. 28 (28) (2014) 04014008.
[22] A.P. Vieira, E.P.D. Moura, L.L. Gonçalves, et al., Characterization of welding defects by fractal analysis of ultrasonic signals, Chaos Solitons Fractals 38 (3) (2008) 748–754.
[23] G. Mozurkewich, B. Ghaffari, T.J. Potter, et al., Resolved ultrasonic attenuation in resistance spot welds: implications for nondestructive testing, Ultrasonics 48 (2008) 343–350.
[24] Hongjie Zhang, Yanyan Hou, Jian Zhao, et al., Automatic welding quality classification for the spot welding based on the Hopfield associative memory neural network and Chernoff face description of the electrode displacement signal features, Mech. Syst. Sig. Process. 85 (2017) 1035–1043.
[25] H.R. Safavi, Conjunctive use of surface water and groundwater: application of support vector machines (SVMs) and genetic algorithms, Water Resour. Manage. 27 (7) (2013) 2623–2644.
[26] Y. Long, Z.J. Du, W.D. Wang, et al., PSO-SVM-based online locomotion mode identification for rehabilitation robotic exoskeletons, Sensors 16 (9) (2016) 1408.
[27] M. Ring, B.M. Eskofier, An approximation of the Gaussian RBF kernel for efficient classification with SVMs, Pattern Recogn. Lett. 84 (2016) 107–113.
[28] M. El-Banna, D. Filev, R.B. Chinnam, Online qualitative nugget classification by using a linear vector quantization neural network for resistance spot welding, Int. J. Adv. Manuf. Technol. 36 (3–4) (2008) 237–248.
[29] P.J.G. Nieto, E. Garíc a-Gonzalo, F.S. Lasheras, Hybrid PSO–SVM-based method for forecasting of the remaining useful life for aircraft engines and evaluation of its reliability, Reliability Eng. Syst. Safety 138 (2015) 219–231.
[30] C.L. Huang, J.F. Dun, A Distributed PSO-SVM Hybrid System with Feature Selection and Parameter Optimization, Elsevier Science Publishers B. V, 2008.
[31] Y. Hou, L. Zhao, H. Lu, Fuzzy neural network optimization and network traffic forecasting based on improved differential evolution, Future Generation Comput. Syst. 81 (2017).
[32] Vladimir Vapnik, The nature of statistical learning theory, Technometrics 38 (4) (1995) 409.
[33] S. Palanisamy, C.R. Nagarajah, K. Graves, et al., A hybrid signal pre-processing approach in processing ultrasonic signals with noise, Int. J. Adv. Manuf. Technol. 42 (7–8) (2009) 766–771.
[34] X. Liu, D. Xiao, Y. Shan, et al., Solder joint failure localization of welded joint based on acoustic emission beamforming, Ultrasonics 74 (2017) 221–232.